Chemical Engineering & Technology Research Article

Maria Ouboukhlik[1,2]
Gilles Godard[2]
Sawitree Saengkaew[2]
Marie-Christine Fournier-Salaün[1]
Lionel Estel[1]
Gérard Grehan[2]

[1]Normandie Université, LSPC-EA 4704, Saint Etienne du Rouvray, France.

[2]Normandie Université, CORIA-UMR 6614, Saint Etienne du Rouvray, France.

Supporting Information available online

Mass Transfer Evolution in a Reactive Spray during Carbon Dioxide Capture

In view of global warming, improvement of CO_2 capture efficiency in addition to carbon valorization has become a major concern. In the last decade, post-combustion capture using amines evolved as one of the most mature technologies for industrial applications. The understanding of mass transfer phenomena is still a challenge for enhancing the absorption step. The mass transfer in a spray column during CO_2 absorption using monoethanolamine as a solvent was characterized. An innovative optical technique called global rainbow technology as a non-intrusive approach to investigate mass transfer is used to measure the amount of CO_2 absorbed in a cloud of droplets in the spray. The CO_2 absorbed flux obtained from experiments is compared to a basic mass transfer model simulated on Comsol Multyphysics®.

Keywords: Carbon dioxide capture, Gas absorption, Global rainbow technique, Mass transfer, Monoethanolamine

Received: November 12, 2014; *revised:* February 02, 2015; *accepted:* April 20, 2015

DOI: 10.1002/ceat.201400651

1 Introduction

Fossil fuels are still the most important energy sources, and the burning of carbon derivatives produces flue gases that contain carbon dioxide (CO_2). CO_2 is the major source of the greenhouse gases (GHG) believed to cause global warming and represents 76.7 % of GHG [1]. Power plants using fossil fuels produce approximately one third of global CO_2 emissions. Post-combustion capture (PCC) in general and the amine-based process in particular are the most technologically mature options to reduce CO_2 from existing power plants. Aqueous solutions of alkanolamines are widely used as solvents to capture acid gases such as CO_2 from flue gas [2]. Khol and Nielsen [3] provided a comprehensive summary of amine-based capture.

Monoethanolamine (MEA) has a high reaction rate with acid gas and its ability to remove even traces of CO_2 has made this chemical absorption one of the most promising technologies [4]. Many authors evaluated the sustainability of CO_2 capture by MEA from incinerator flue gas using packed columns [5, 6]. It is clear that a significant improvement in the separation step is required, with high efficiency, compactness, and operationally flexible contactors. So far, little attention is given to spray columns for CO_2 capture. The main advantages of this type of contactors are to optimize the exchange area between the two phases and significantly reduce the pressure drop for the gas. Spray columns also offer a very basic operation and equipment compared to packed columns, with no limits due to flooding or excessive foaming in the column. These contactors are widely applied for SO_2 capture and have been studied in terms of capture efficiency with various solvents such as sodium hydroxide, ammonia, and amines [7–12].

An optical and non-intrusive technique, namely, the global rainbow technique (GRT), is applied to measure mass transfer evolution along a spray column at different heights. This technique is based on measuring the refractive index of the droplets. During CO_2 capture, the concentration inside the droplets in a spray changes, leading to a density evolution and thus, a refractive index evolution. The density of the droplets during the chemical absorption depends on temperature and concentration of absorbed CO_2. Therefore, the determination of the refractive index of droplets by GRT is a measurement of the CO_2 absorption extent. In addition to GRT, phase Doppler anemometry (PDA) is used to characterize size and velocity distributions in the spray.

2 Mass Transfer Theory

The reaction between CO_2 and MEA (RNH_2) has been described in many studies. According to Satori and Savage [13], the carbamate formation is considered to be the main reaction between CO_2 and MEA. The reversible reaction is neglected due to the temperature of the measurement volume in this study.

Correspondence: Maria Ouboukhlik (maria.ouboukhlik@insa-rouen.fr), Normandie Université, LSPC-EA 4704, 76800 Saint Etienne du Rouvray, France.

The reaction with a rate constant k[1)] can be expressed as follows:

$$CO_2 + 2RNH_2 \xrightarrow{k} RNH_3^+ + RNHCOO^- \quad (1)$$

Regarding the reaction rate dependence, the reaction kinetic is known to be first order with respect to both reactants CO_2 and MEA [14].

The reaction rate is expressed as follows:

$$r = k\,[CO_2]\,[MEA] \quad (2)$$

To predict the mass transfer during CO_2 capture by MEA droplets, mass transfer parameters are required. In this study, the values of rate constant k are obtained at different temperatures with the correlation provided by Hikita et al. [15]. The CO_2 diffusion coefficient in aqueous MEA solution is taken from Versteeg and Van Swaaij [16] as a function of temperature while the MEA diffusion coefficient is reported in [17]. Finally, CO_2 solubility is expressed with Henry's constant as studied by Versteeg and Van Swaaij [16] and correlated with temperature by Maceiras et al. [18].

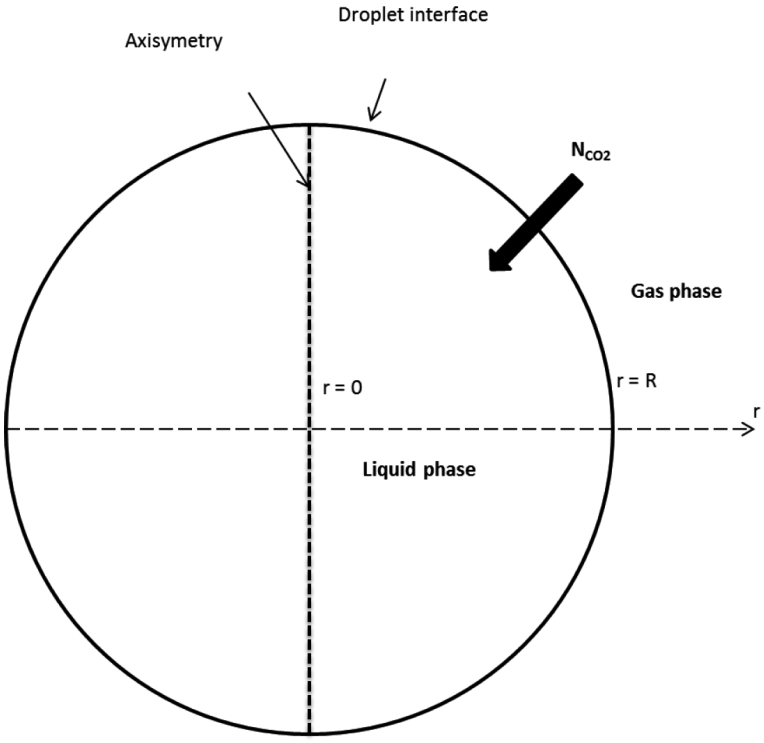

Figure 1. Illustrating sketch of the modeled droplet.

3 Mass Transfer Prediction

In a spray column, the droplets generated by an ultrasonic nozzle can be modeled as a spherical droplet with a diameter corresponding to the mean diameter of the spray. This is possible if there is no droplet coalescence or distortion. Thus, a perfectly axisymmetric and spherical droplet is considered in this model (Fig. 1). According to Elperin and Fominykh [19], a spherical shape is observed up to a Reynolds number of 300, which corresponds to a water droplet of 1 mm falling in air. Beyond this limit, the drop oscillates and loses its sphericity.

3.1 Assumptions

The droplet is supposed isothermal and all transfer parameters presented above are taken at a constant droplet temperature. The droplet is in contact with pure CO_2 atmosphere. Furthermore, the droplet is assumed rigid without internal circulation; this assumption is possible for a small diameter. Indeed, Clift et al. [20] reported that water droplets smaller than 1 mm falling in air can be considered as rigid sphere. The droplet in this model is assumed motionless; this assumption is verified since the Sherwood number of the droplet is about 3.2 leading to a gas film close to 30 % of the droplet diameter. MEA and CO_2 are the only reactants and have a global rate order of 2. Reversibility of the reaction is not taken into account because the droplet temperature does not exceed 50 °C.

The aim of this model is to obtain the flux of CO_2 absorbed into a rigid spherical droplet. Fig. 1 displays an axisymmetric droplet in a gas phase. The droplet is initially an aqueous solution of 30 wt % MEA in a pure CO_2 atmosphere. For further details refer to the Supporting Information.

3.2 Equations

The mass balance on a differential element is done in spherical coordinates for each species on the axisymmetric droplet:

$$\text{Inlet} - \text{outlet} = \operatorname{div}(D_{\text{species}}\overrightarrow{\nabla[\text{species}]}) = D_{\text{species}}\left(\frac{\partial^2[\text{species}]}{\partial r^2} + \frac{2}{r}\frac{\partial[\text{species}]}{\partial r}\right) \quad (3)$$

The mass production source term is linked to the kinetic of the reaction which is negative for CO_2 and MEA.

The mass balance on CO_2 and MEA using Fick's law is then:

$$D_{CO_2}\left(\frac{\partial^2[CO_2]}{\partial r^2} + \frac{2}{r}\frac{\partial[CO_2]}{\partial r}\right) = k\,[CO_2][MEA] + \frac{\partial[CO_2]}{\partial t} \quad (4)$$

$$D_{MEA}\left(\frac{\partial^2[MEA]}{\partial r^2} + \frac{2}{r}\frac{\partial[MEA]}{\partial r}\right) = 2\,k\,[CO_2][MEA] + \frac{\partial[MEA]}{\partial t} \quad (5)$$

1) List of symbols at the end of the paper.

3.3 Boundaries and Initial Conditions

At gas liquid interface, there is equilibrium between CO_2 in gas and liquid phase. The droplet is in pure CO_2 atmosphere and mass transfer resistance is neglected. The equilibrium assumption can be modeled by Henry's law according to Eq. (6). On the other hand, the MEA molecules are assumed nonvolatile imposing a null flow on the gas liquid interface. Thus, boundaries conditions can be expressed as follows:

$$[CO_2]_{r=R} = He_{CO_2} P_{CO_2} \quad (6)$$

MEA nonvolatility is expressed with the MEA concentration gradient at the liquid gas interface:

$$\left.\frac{\partial[MEA]}{\partial r}\right\}_{r=R} = 0 \quad (7)$$

At $r = 0$, the continuity of concentration in the axisymmetric droplet is imposed.

Initial conditions: Originally, the droplet is only composed of MEA molecules mixed with water. The initial MEA concentration used in the model is the concentration of an aqueous solution of 30 wt % MEA, about 5000 mol m^{-3}, while there is no CO_2 in the droplet at $t = 0$.

$$[MEA]_0 = 5000 \text{ mol m}^{-3} \quad (8)$$

$$[CO_2]_0 = 0 \text{ mol m}^{-3} \quad (9)$$

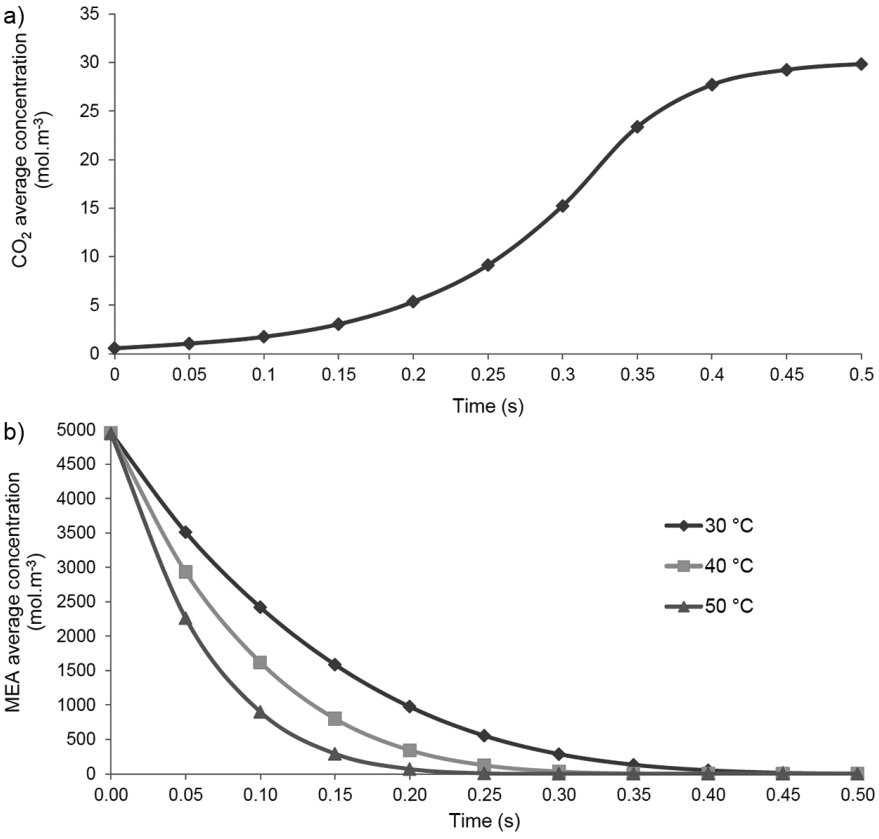

Figure 2. (a) Average CO_2 concentration as a function of time for a 50-μm droplet at 40 °C. (b) Average MEA concentration in function of time at different droplet temperatures.

3.4 Simulation Results

Eqs. (4)–(7) are solved numerically with Comsol Multiphysics® 4.2a software. The finite element method (FEM) is used to solve the boundary value problem in 2D axisymmetric geometry.

3.4.1 Average MEA Concentration in the Droplet

CO_2 barely exists inside the droplet. Simulation demonstrates that CO_2 is only present at the gas liquid interface ($r = R$) since it is consumed very quickly by MEA as indicated in Fig. 2 a. This paragraph presents the average MEA concentration in the droplet over time. Fig. 2 b shows the MEA average concentration inside a droplet of 50 μm diameter at different temperatures over time, pointing to two important results.

First, the cancellation of the different curves represents chemical saturation of the droplet since more MEA is available. This saturation time is important to design spray towers and corresponds to a minimum contact time needed to complete the chemical absorption, thus the needed height, knowing the average velocity of the droplets.

In addition, the curves also demonstrate that MEA consumption strongly depends on temperature. Thus, for a temperature of 30 °C, the saturation of the drop occurs at 0.45 s after the generation of the droplet from the orifice while for a droplet at 50 °C, the chemical absorption ends at 0.25 s. For a droplet average velocity of 1 m s^{-1}, a height of 45 cm is required to completely saturate a spray at 30 °C, while only 25 cm are needed for drops at 50 °C.

3.4.2 CO_2 Absorbed Flux in the Droplet

The CO_2 absorbed flux (mol $m^{-2}s^{-1}$) is obtained from Fick's law according to the following expression:

$$N_{CO_2} = D_{CO_2} \left.\frac{\delta[CO_2]}{\delta r}\right]_{r=R} \quad (10)$$

It corresponds to the amount of CO_2 that has been transferred from the gas phase to the liquid phase. CO_2 absorbed flux is plotted in Fig. 3 a for different temperatures and for a droplet of 50 μm in diameter. The saturation of the droplets

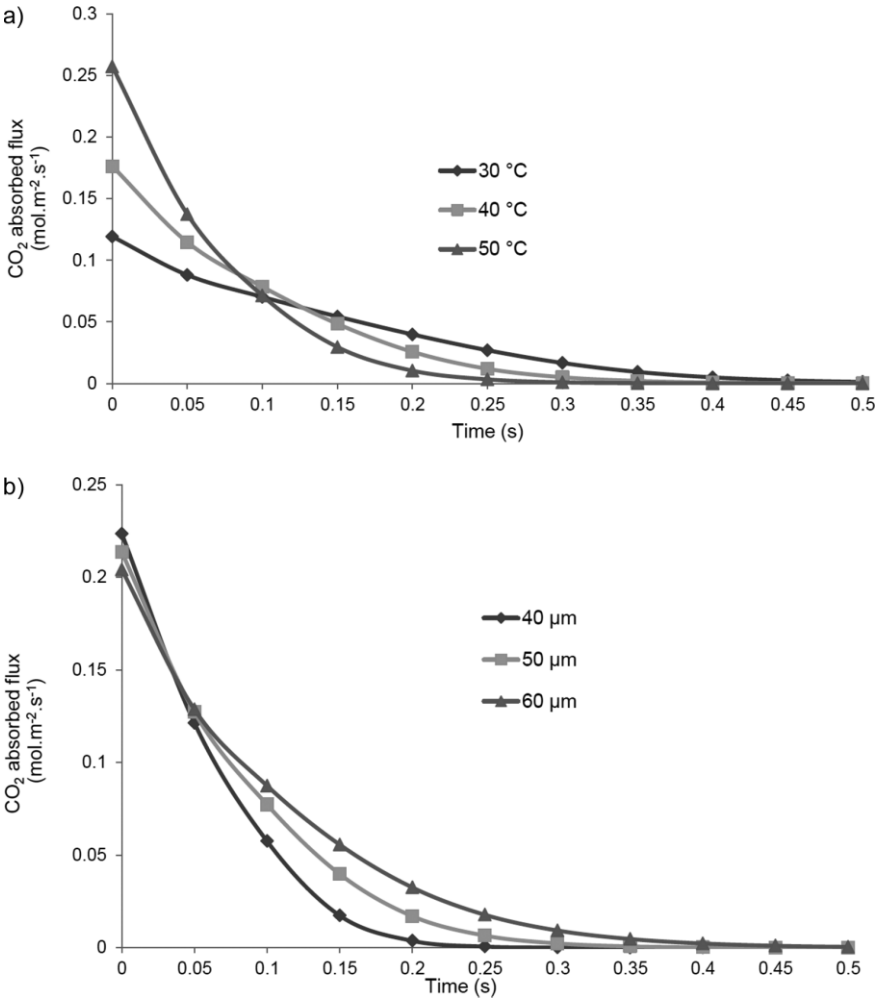

Figure 3. Flux of CO_2 absorbed as function of time (a) for a 50-µm droplet at different temperatures, (b) for different droplet diameters at 45 °C.

(N_{CO_2} = 0) for each curve is in good agreement with the total consumption of MEA in the droplet (Fig. 2 b).

3.4.3 Dependence on Diameter

In order to compare the model to the experiment, the temperature chosen is the average temperature of the measured volume (see experimental setup), which is 45 °C. Thus, this part is devoted to CO_2 absorbed flux evolution during time for a temperature at 45 °C at different droplet diameters. Results in Fig. 3 b illustrate the influence of the droplet diameter on CO_2 absorbed cancellation, which corresponds to the saturation of the droplets. Indeed, smaller droplets are quickly saturated because of the lower MEA quantity available inside. CO_2 absorbed flux values obtained in this simulation section also depend on mass transfer parameters, specially Henry's constant, used from literature.

4 Optical Measurement Theory

4.1 Global Rainbow Technique (GRT)

4.1.1 Standard Rainbow

In ray optics, a rainbow corresponds to an extremum of deviation [20] characterized by a local peak of intensity. When a light ray is beamed on a spherical droplet, first an external reflection on the droplet surface occurs ($p = 0$), followed by two refractions on both sides of the droplet ($p = 1$) and a refraction/reflection/refraction which corresponds to p = 2, as demonstrated in Fig. 4 a.

The maximum intensity is located close to the extremum of p = 2, and the interference between these rays creates the main rainbow supernumerary peaks. In wave optics, diffraction must be taken into account. Therefore, the rainbow's shape and the angular location of the maximum intensity depend not only on the refractive index, but also on the droplet size. The interference between different kinds of 'rays', i.e., externally reflected, n times internally reflected, etc., must be noted. The Airy theory and optical geometry give a good idea of what represents a rainbow. However, the Lorenz-Mie theory provides an exact solution for the problem considered. Application of the rainbow to measure the droplet refractive index, i.e., temperature and/or composition, has been proposed by Roth et al. [21].

The main difficulties when using this technique on individual droplets are lines of identical droplets deriving from the ripple structure created by the interference between externally and internally reflected light, and its sensitivity to droplet nonsphericity. Recent progress in signal processing [22] permits good results to be obtained on lines of identical droplets and individual droplets which are measures of both temperature and evaporation rate.

4.1.2 Global Rainbow

To avoid difficulties due to nonsphericity and ripple structure, Van Beeck et al. [23] have introduced the GRT. In their approach, the rainbows created by droplets crossing the volume for measurement during a time interval are added together, generating a global rainbow. This global rainbow is characterized by smooth behavior, thus the ripple structure is

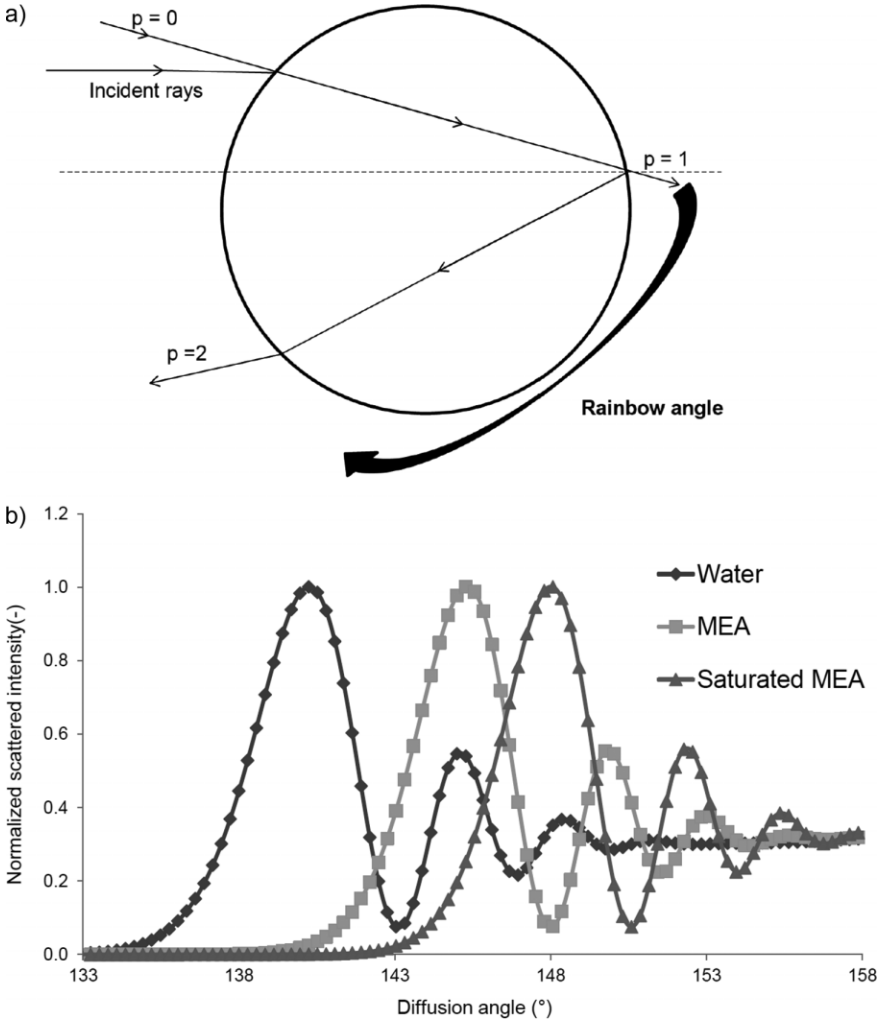

Figure 4. (a) Illustrating sketch of geometrical optics, (b) computed global rainbows with Nussenzveig's theory.

suppressed. Also, the GRT demonstrated robustness to non-sphericity [24].

The Lorenz-Mie theory is the most rigorous theory to describe the light around the rainbow angle, but also the most time-consuming and nonlinear on diameter and refractive index. A code has been developed by Saengkaew et al. [25] based on Nussenzveig's theory combined with Non Negative Least Square (NNLS) and minimization. Nussenzveig's theory takes into account the interference between the first internal reflected light (p =v2) and externally reflected ($p = 0$). NNLS researches the best size distribution for a given refractive index. The refractive index is extracted by minimizing the distance between the computed intensity profile and the measured intensity. This inversion algorithm is used in this work to measure the average refractive index value with the associated size distribution. It has been shown that the Nussenzveig theory provides the best choice in terms of accuracy and computation efficiency [26]. The refractive index values can then be extracted from the absolute angular position. The recorded signal corresponds to the contribution of many individual rainbow signals. This superimposition of signals leads to a steady rainbow pattern and gives an average-weighted refractive index which provides valuable information about temperature and/or composition of droplets [21–29].

A computed normalized rainbow using Nussenzveig's theory is displayed in Fig. 4 b which displays the rainbow pattern of three clouds of droplets. The droplets' average diameter is 50 µm. The first curve corresponds to water droplets with a refractive index of 1.3330; water is presented for a reference illustration. The second curve corresponds to MEA droplets with a refractive index of 1.3710 and the third one to saturated MEA droplets, i.e., fully loaded with CO_2, with a refractive index of 1.3930.

The rainbow angle of water droplets is 137.92° while that of clean MEA is 143.14° and of saturated MEA 145.91°. This indicates that measuring the rainbow angle with a good precision is a satisfying way to reach the absorption extent.

4.2 PDA Theory

PDA is an optical non-intrusive technique for measuring velocity and size of one droplet. From a series of such elementary measurements, the correlation size/velocity can be extracted as well as velocity and size distribution. PDA was developed and first utilized as an indication of particle size in 1975 [30]. It is an extension of laser Doppler velocimetry (LDV) in which an optical probe is produced by interfering Gaussian laser beams. The light scattered by a moving droplet is collected by detectors. The phase shift between a pair of signals is related to the diameter of the droplet, assumed to be spherical. The location of measurement in a spray is defined by the probe volume which is an intersection of the laser beams. The velocity distribution is deduced from the frequency of scattered light signals.

5 Experimental

5.1 CO_2 Capture Facility

In general, spray columns are cylindrical; however, for optical diagnostics, a plane optical window is recommended. Therefore, the gas absorption setup consists of a stainless-steel cylinder on top of a polycarbonate chamber (Lexan®). Fig. 5 illustrates the experimental setup.

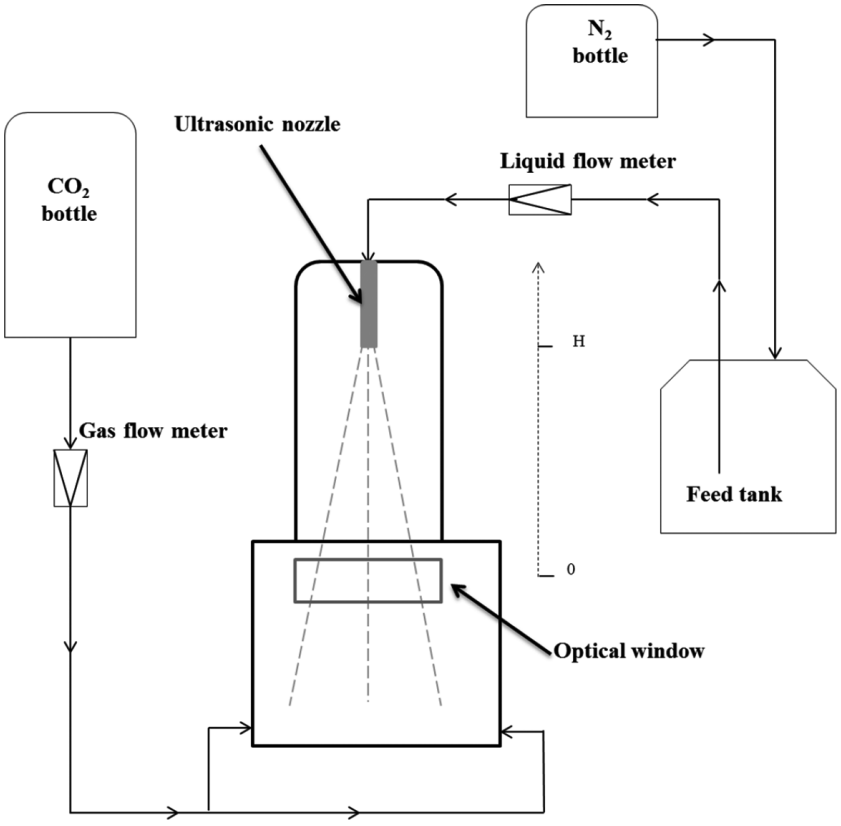

Figure 5. Process diagram of a CO_2 capture facility.

The chamber is fitted with an optical window made of glass on the front. The height of the cylinder is 30 cm and the diameter is 18 cm. This choice of column diameter is made to prevent wall liquid dripping. The polycarbonate chamber, made of Lexan®, is 30 cm high, 20 cm deep, and 30 cm large. An ultrasonic nozzle is placed on the top of the column and creates a cloud of droplets with a frequency of 40 kHz. The diameter and the velocity of the droplets depend on the liquid flow rate. The ultrasonic nozzle is provided by ACIL (model US630-0499G).

The ultrasonic spray nozzle is connected to a feed tank loaded with 30 wt % aqueous MEA. The feed tank is made of stainless steel and is connected with a nitrogen bottle in order to create a liquid flow. The pressure inside the tank is about 2 bar for a volume of 5 L. The liquid flow is controlled with a flow meter provided by Brooks (model 2-65B). In order to perform measurements along the spray at different heights, the top of the column is designed to be removable, so the height of the column can be varied.

The gas inlet is located at the bottom of both sides of the chamber. This brings the gas and liquid into countercurrent exchange. The gas, after CO_2 absorption, is carried out through the top of the column to an event while the rich solution is sent to the liquid receiver located at the bottom of the column. The laser for GRT measurements is beamed through the optical glass window located in the spray column and encounters the spray perpendicularly.

5.2 Optical Setup for GRT

The optical setup is displayed in Fig. 6 and consists of:

- a continuous laser source with a wavelength of 589 nm and power of 50 mW, provided by Shanghai Dream Lasers Technology Co. Ltd (model SDL-589-050T)
- a first collecting lens with 80 mm diameter and 150 mm focal length
- a second lens with 80 mm diameter and 200 mm focal length
- a spatial filter with 1 mm diameter
- a CCD camera from Kappa (model DX 2 HC-FW).

The first collecting lens creates an image of the control volume on a spatial filter. The spatial filter (or pinhole) is then located on the image plane of the first lens. The second collecting lens generates an image of the first lens focal plane on the detector. This optical setup with a spatial filter allows only the light scattered by the particles located in the control volume in the spray (1 mm^3) and organized by the scattering angle to be collected.

5.3 PDA Setup

The PDA setup is provided by Dantec Dynamics® and consists of an emitting part, a receiving part, and a signal processor. The emitting part includes a system of two 1-W diode lasers, model Genesis MX 488-1000 SLM and Genesis MX 532-1000 SLM. The laser wavelengths are 488 and 532 nm. The beam combination system is manufactured by Dantec Dynamics®. A

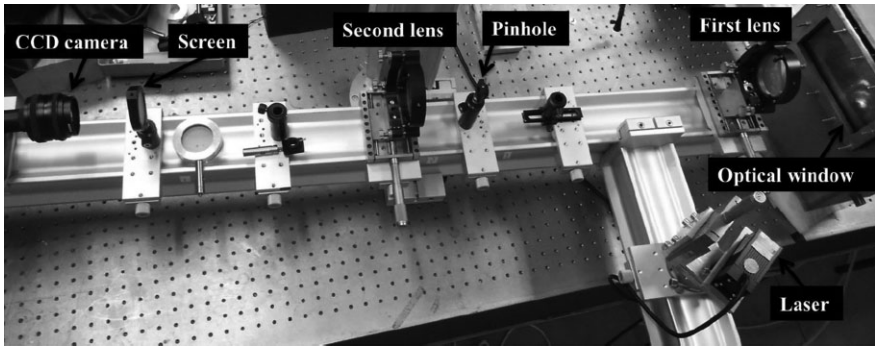

Figure 6. Photo of the GRT optical bench.

2D 85-mm fiber optic transducer (Dantec Dynamics® 60X 83) is used to create the measurement volume. The laser coupling is realized by Dantec FiberFlow optical system. The emitting focal length is 350 mm; the beam diameter is 2.2 mm while the beam spacing is 40 mm.

The receiving part involves a signal collecting unit located in the forward direction at 30°. This angle has been chosen to be in the scattering mode dominated by first-order refraction. The receiving part consists of a 112-mm diameter Dual PDA probe. The focal length of the receiver is 310 mm. The range of measurable diameters for this configuration runs from about 5 to 225 µm. The collected signal is transmitted by optical fibers to the detector unit and is processed by a BSA P80 processor. The measurement accuracy of the velocity is about 5 % and of the size about 10 % of the measured value.

5.4 Experimental Procedure for Mass Transfer Measurement by GRT

The experiment starts by introducing the gas phase which is pure CO_2 at the desired flow rate. To make sure that the gas concentration is uniform inside the column, the solvent is sprayed after four times the time needed to fill up the column. Once the system reaches steady state after injecting the spray, the laser is beamed on the volume to be measured by GRT. The top of the column is adjusted for each experiment to reach the desired height. When finishing the GRT experiment, a temperature measurement is made at the same volume beamed by the laser by using a thermocouple. This allows a corresponding temperature with each GRT measurement. Tab. 1 summarizes the operating conditions.

Table 1. Operating conditions during experiments in the column.

Solvent composition [wt % MEA]	30
Gas phase	Pure CO_2
Pressure inside the column [kPa]	1013
Average temperature of measurement volume [°C]	45
Column height [cm]	5–25

6 Results

6.1 Preliminary Results: Size and Velocity Distribution in the Spray

There are different types of nozzles that can generate a spray such as plain orifice nozzles, air-blast nozzles, effervescent nozzles, hydraulic nozzles etc. A spray generated with an ultrasonic nozzle is the most suitable for mass transfer experiments because of its low droplet density and significantly low average diameter and average velocity. The low density allows all the droplets in the spray to be in contact with the same CO_2 concentration. The low size and velocity distribution leads to a low Reynolds number and thus an absence of droplet oscillation, distortion, strong internal circulation etc.

In order to compare the GRT measurement to the model results presented above, velocity and size distribution of the spray must be known. Therefore, PDA is used to measure the arithmetic mean diameter and the mean velocity at different positions of the spray. Fig. 7 demonstrates the evolution of the average diameter and the average velocity along the spray. Results shows that the arithmetic average diameter and velocity oscillate within the PDA measurement accuracy.

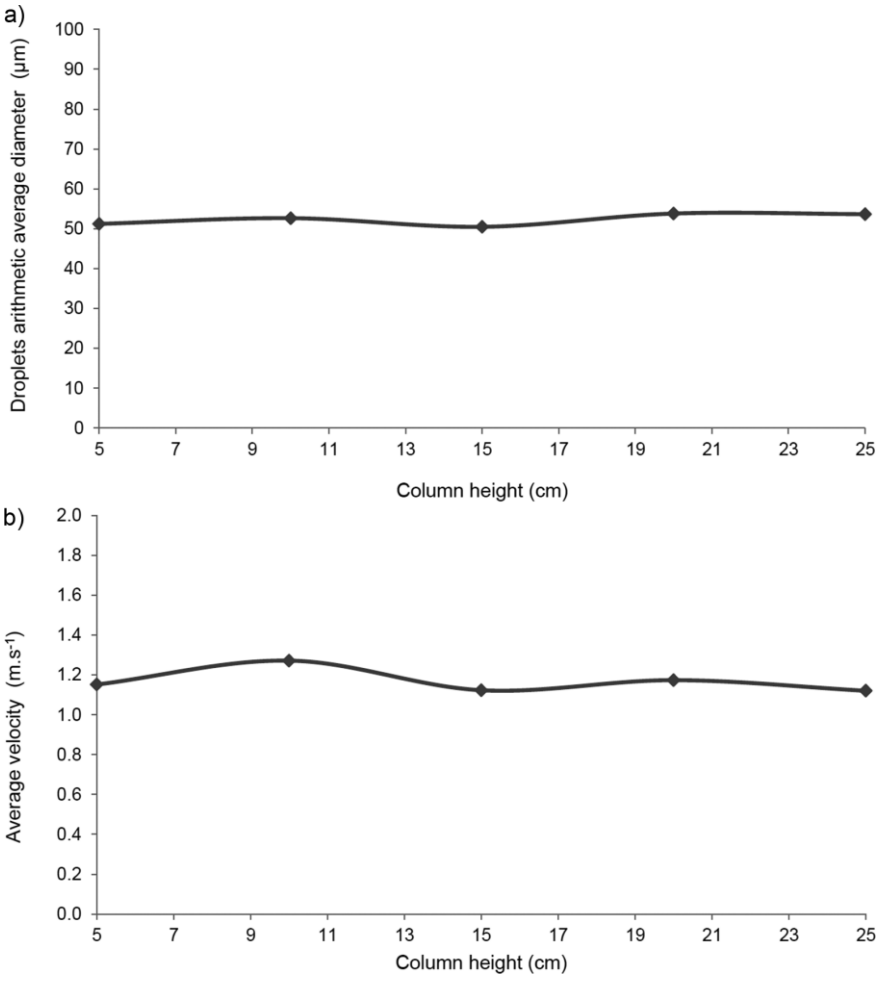

Figure 7. Evolution of (a) arithmetic mean diameter with column height, (b) mean velocity of a droplet with column height.

6.2 Mass Transfer Measurement

In order to measure the CO_2 absorbed concentration along the column, four steps are required. The first step is to take rainbow pictures at the desired height when absorption reaches steady state. The second step is devoted to optical calibration in order to obtain from the rainbow pictures the scattered intensity at each diffusion angle. The third step uses an inversion code to extract refractive index values from the scattered intensity/diffusion angle. Finally, the last step is to acquire from the average refractive index the corresponding concentration of CO_2 absorbed at a known temperature; therefore, a correlation of refractive index with temperature and CO_2 absorbed concentration is needed.

6.2.1 Rainbow Pictures

For each experiment at a defined height, more than 200 rainbow pictures are taken. Fig. 8 a presents the rainbow pictures obtained for a 30 wt % aqueous MEA solution with and without CO_2 chemical absorption. The global rainbow is characterized by a peak of intensity. Each individual rainbow created by a droplet in the volume for measurement located in the spray is the result of interference between one-time internally reflected rays in this droplet. The global rainbow is created by the addition of individual rainbows generated by the particles located in a section of the spray. The location of this global rainbow is a function of the refractive index of the droplets.

The global rainbow angle increases with the refractive index. Fig. 8 a shows that the main rainbow shifts to the right after CO_2 absorption which proves that CO_2 absorption is happening.

6.2.2 Optical Calibration

The optical calibration is a correlation between each angle and the corresponding pixel on the camera. Therefore, a mirror on a goniometer is used. The laser is beamed on the mirror at a defined angle read from the goniometer, and the reflected spot on the camera gives the corresponding pixel or intensity. By using this pixel/angle calibration, the normalized scattered intensity from the photos can be plotted versus the scattering angle for the CO_2-loaded MEA. Fig. 8 b indicates the scattered normalized intensity at each diffusion angle from the rainbow photo displayed in Fig. 8 a. The plot shows that the rainbow angle varies from 142.5° for non-loaded MEA to 145.5° for loaded MEA. When the refractive index of the particle increases, the rainbow moves toward a larger scattering angle to the right. The opposite occurs when the refractive index decreases.

6.2.3 Refractive Index Extraction

As previously explained, an inversion code using Nussenzveig's theory is applied, and the average refractive index is extracted from the normalized scattered intensity and the scattering angle. For this, a first value of the refractive index is estimated from the global rainbow position by using the geometrical optics law. With this geometrical refractive index in hand, a matrix is then computed by Nussenzveig's theory. Each line in the matrix corresponds to the scattering intensity in a given direction and each column is associated with the scattered intensity for a given diameter. A size distribution is then computed using the NNLS method. The rainbow matrix is then recomputed to minimize the distance between the measured global rainbow and the recomputed global rainbow in order to obtain the best values for the refractive index and size distribution.

Fig. 9 a illustrates the evolution of the average refractive index at different heights in the spray from 0 to 25 cm. The

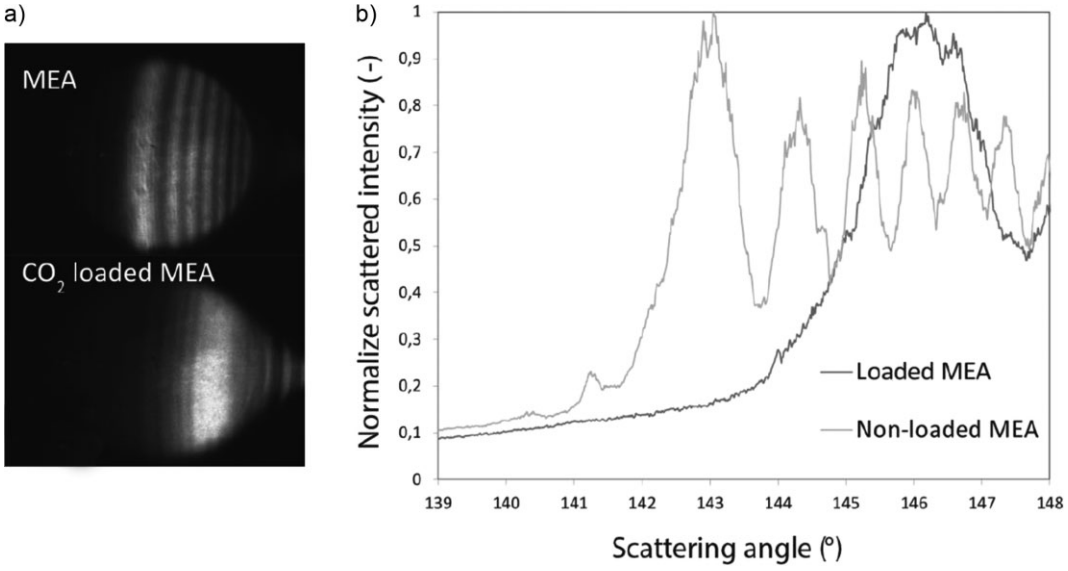

Figure 8. (a) Rainbow photo before and after CO_2 absorption, (b) normalized scattered intensity versus the diffusion angle corresponding to the photo displayed in (a).

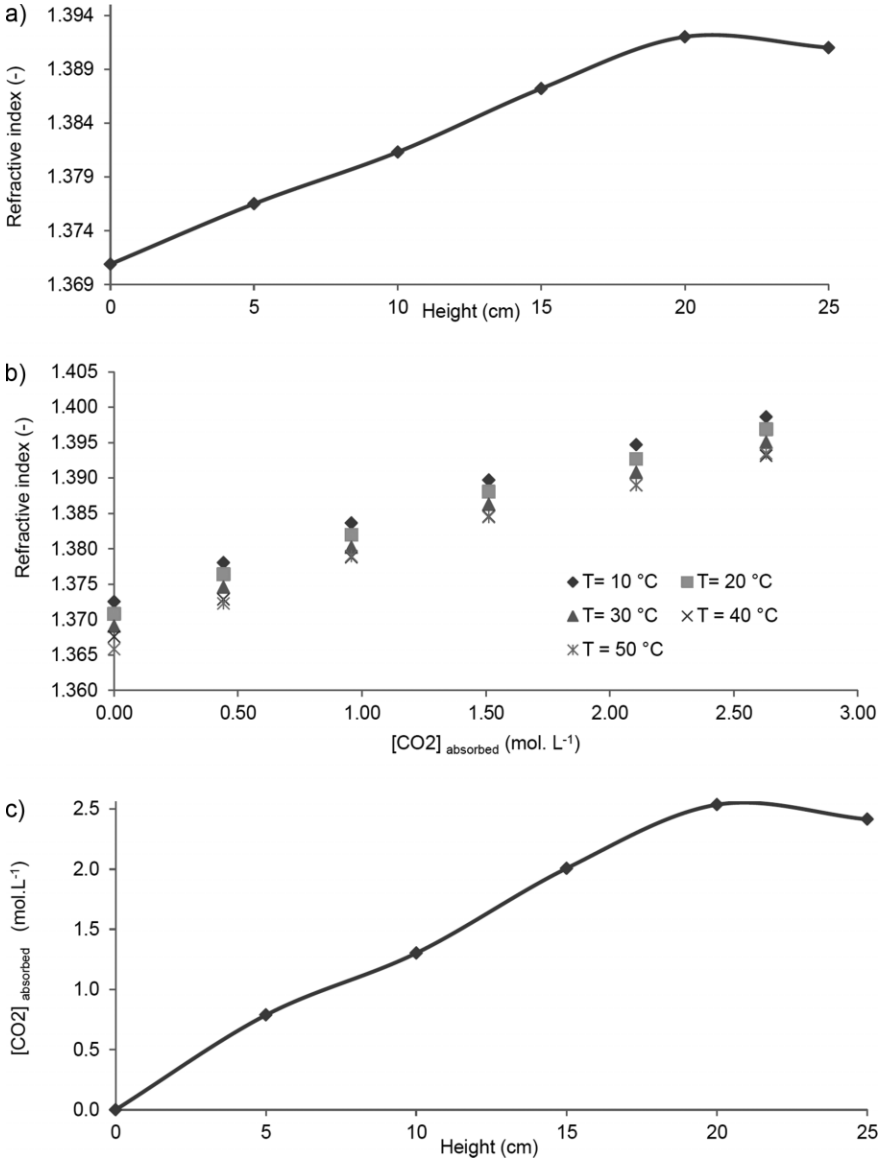

Figure 9. (a) Evolution of the average refractive index with column height; (b) calibration curves for CO_2 absorbed concentration; (c) evolution of the CO_2 absorbed concentration with the column height.

increase of the refractive index with height shows that the absorption occurs until a height between 20 cm.

6.2.4 Calibration for CO_2 Absorbed

To find the CO_2 absorbed concentration from the average refractive index, a calibration is needed. The refractive index changes with density, which depends on temperature and concentrations in the solution. Thus, 30 wt % was loaded with five different concentrations of CO_2 in a stirred cell. Samples at each concentration of CO_2 absorbed were taken. The refractive index of these samples was measured with a standard refractometer (Anton Paar, model Abbemat 300) at different temperatures from 10 °C to 50 °C. Then a correlation of the refractive index in function of temperature and CO_2 absorbed concentration is obtained; see Fig. 9 b. The $[CO_2]_{abs}$ accuracy of this calibration is 0.06 mol L^{-1}. This accuracy takes into account the error from the stirred-cell experiment, fitting data, and refractive index measurement with the Abbemat refractometer.

Taking this calibration and the measured temperature in the probe volume, a profile of CO_2 absorbed concentration is obtained with the column height; see Fig. 9 c. The CO_2 absorbed concentration accuracy from only the GRT measurement is 0.04 mol L^{-1}, leading to a total $[CO_2]_{abs}$ accuracy of 0.1 mol L^{-1} while taking into account the calibration error contribution of 0.06 mol L^{-1}; see above.

This result shows that CO_2 absorption occurs from the outlet of the injector until a height of 20 cm. Then, the CO_2 absorbed concentration decreases by 0.1 mol L^{-1} which is the experimental error.

7 Discussion and Conclusions

7.1 Comparison with the Model

The concentration of CO_2 absorbed inside the droplet $[CO_2]_{abs}$ corresponds to the moles of CO_2 transferred from the gas phase to the droplet divided by the droplet volume. The quantity of CO_2 transferred inside the droplet (volume $V_{droplet}$ and a surface $S_{droplet}$) during a time t corresponds to CO_2 absorbed flux (Eq. (6)). The measured values of diameter and velocity by PDA technique (Fig. 8) give arithmetic means of both parameters along the column and are used to calculate CO_2 absorbed flux according to Eqs. (11) and (12).

$$[CO_2]_{abs} = \frac{n_{abs}}{V_{droplet}} = N_{CO_2} \times \text{time} \times \frac{S_{droplet}}{V_{droplet}} = N_{CO_2} \times \text{time} \times \frac{6}{d_{droplet}} \quad (11)$$

The measured N_{CO2} accuracy taking into account GRT and PDA accuracies is about 0.03 mol $m^{-2}s^{1}$.

The measured CO_2 absorbed concentration by GRT is transformed to an average CO_2 absorbed flux between two heights according to the following expression:

$$\overline{N_{CO_2}} = \frac{\Delta[CO_2]_{asborbed}}{\Delta t}\frac{V_{droplet}}{S_{droplet}} = \frac{\Delta[CO_2]_{asborbed}}{\Delta H}\frac{v_{droplet}\,V_{droplet}}{S_{droplet}} \quad (12)$$

The CO_2 absorbed flux is compared to the flux simulated on Comsol Multiphysics® for three equivalent droplet diameters of 40, 50, and 60 µm (Fig. 10). This range of diameter corresponds to 50 µm ± 20 % which is larger than 10 % precision on diameter announced by PDA measurement.

In Fig. 10, three zones can be highlighted. In the first range until 0.1 s, i.e., about 10 cm, the experimental flux is in a good agreement with the simulated ones. Indeed, the flux at the beginning of the experiment is higher. This is explained by the MEA diffusion which brings available MEA at the interface in order to react with CO_2.

In the second range from 0.1 to about 0.19 s, i.e., from 10 to 20 cm, the experimental flux decreases as predicted by the simulation. However, the experimental flux remains higher than the simulated one. An increase of the experimental mass flux can be explained by a raise of temperature inside the droplets, leading to an acceleration of mass transfer. However, this deviation falls within the precision of mass transfer measurement by GRT being about 0.03 mol $m^{-2}s^{-1}$ for the closest simulated curve at 60 µm diameter.

In the last range from 20 to about 25 cm, the cancellation of the experimental curve and the simulated one are in good agreement, at about 0.2 s. This means that the absorption is finished at 20 cm and saturation does not depend on the droplet diameter. However, the experimental flux becomes negative at 0.21 s. A negative mass transfer could be due to CO_2 desorption while this phenomenon is not taken into account in the model, but the deviation also falls within the precision of mass transfer measurement by GRT.

8 Conclusions

CO_2 absorbed flux during CO_2 capture was successfully measured by the global rainbow technique which is its first application for transient mass transfer evolution in a chemical absorption. This measured flux was compared to a basic mass transfer model for three equivalent droplet diameters, namely, 40, 50, and 60 µm. GRT mass transfer measurement indicated that the CO_2 absorbed flux is higher at the beginning of the absorption according to the simulation. In the middle of the absorption, the experimental flux is higher than the computed one, but the deviation mostly falls within with the GRT measurement accuracy of about 30 % for the 60-µm droplet diameter flux. At the end of the absorption experiment, the droplets' saturation time or height agreed well with the simulation.

Acknowledgment

The authors gratefully acknowledge the financial support provided by "La Région Haute Normandie" and the E3C3 project (No. 4274), which was selected by the European INTERREG IV France (Channel) – England Cross-border Cooperation Program and co-financed by ERDF. Authors also thank Carole Gobin for her contribution during PDA experiments.

The authors have declared no conflict of interest.

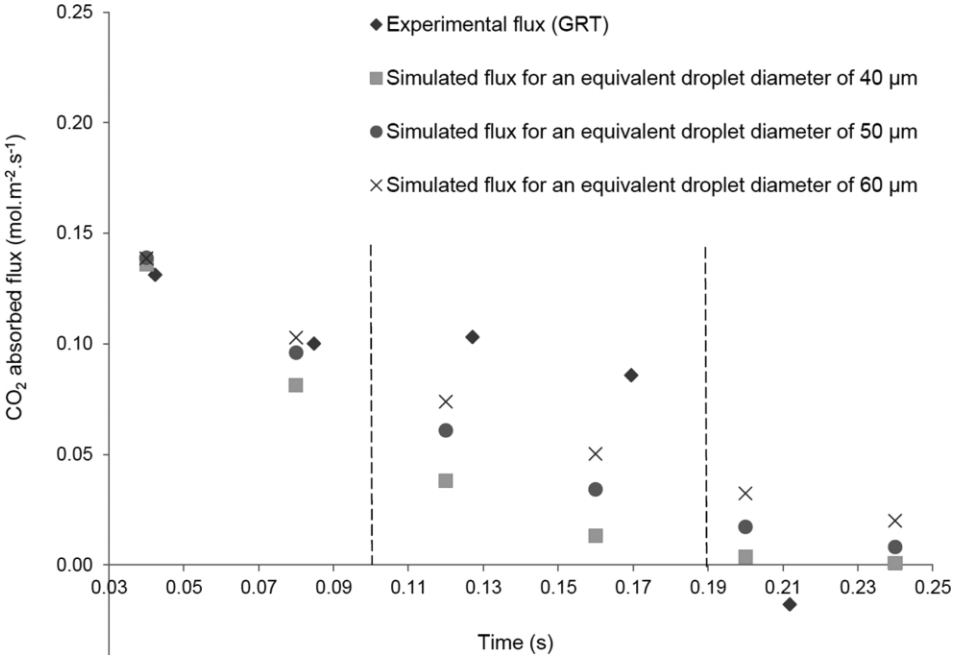

Figure 10. Experimental CO_2 absorbed flux in comparison to the simulated flux for three equivalent droplet diameters of 40, 50, and 60 µm.

Symbols

$[CO_2]$	[mol m^{-3}]	CO_2 concentration inside the droplet
$[CO_2]_0$	[mol m^{-3}]	CO_2 initial concentration inside the droplet
$[CO_2]_{abs}$	[mol m^{-3}]	quantity of CO_2 absorbed (mole) from the gas phase to the droplet divided by the droplet volume (or CO_2 absorbed concentration)
D_i	[m^{2}s^{-1}]	diffusion coefficient of the species *i*
$d_{droplet}$	[m]	droplets arithmetic mean diameter
He_{CO2}	[mol m^{-3}MPa^{-1}]	CO_2 Henry constant in 30 % aqueous MEA
k	[m^{3}mol^{-1}s^{-1}]	reaction rate constant
[MEA]	[mol m^{-3}]	MEA concentration inside the droplet
$[MEA]_0$	[mol m^{-3}]	MEA initial concentration inside the droplet
N_{CO2}	[mol m^{-2}s^{-1}]	CO_2 absorbed flux
P_{CO2}	[Pa]	CO_2 partial pressure
R	[m]	droplet radius
$S_{droplet}$	[m^2]	droplet area
T	[K]	temperature
t	[s]	time
$v_{droplet}$	[m s^{-1}]	droplets arithmetic mean velocity
$V_{droplet}$	[m^3]	droplet volume

Greek letter

μ_i	[Pa s]	dynamic viscosity of the species *i*

Abbreviations

FEM	finite element method
GHG	greenhouse gases
GRT	global rainbow technique
MEA	monoethanolamine
NNLS	non-negative least square
PCC	post-combustion capture
PDA	phase Doppler anemometry
RNH_2	monoethanolamine
RNH_3^+	protonated MEA
$RNHCO^-$	carbamate

References

[1] Intergovernmental Panel on Climate Change, *4th Assessment Report*, Switzerland **2007**.

[2] F. Lecomte, P. Broutin, E. Lebas, *Le Captage de CO_2*, Technip, Paris **2010**.

[3] A. Kohl, R. Nielsen, *Gas Purification*, 5th ed., Gulf Publishing Company, Houston, TX **1997**.

[4] A. Aboudheir, P. Tontiwachwuthikul, A. Chakma, R. Idem, *Can. J. Chem. Eng.* **2003**, *81 (3–4)*, 604–612. DOI: 10.1002/cjce.5450810336

[5] D. DeMontigny, P. Tontiwachwuthikul, A. Chakma, *Ind. Eng. Chem. Res.* **2005**, *44 (15)*, 5726–5732. DOI: 10.1021/ie040264k

[6] I. Aouini, A. Ledoux, L. Estel, S. Mary, *Oil Gas Sci. Technol.* **2014**, *69 (6)*, 1091–1104. DOI: 10.2516/ogst/2013205

[7] I. Taniguchi, H. Yokoyama, K. Asano, *J. Chem. Eng. Jpn.* **1999**, *32 (1)*, 145–150. DOI: 10.1252/jcej.32.145

[8] I. Taniguchi, Y. Takamura, K. Asano, *J. Chem. Eng. Jpn.* **1997**, *30 (3)*, 427–433. DOI: 10.1252/jcej.30.427

[9] K. C. Mehta, M. M. Sharma, *Br. Chem. Eng.* **1970**, *15 (11)*, 1440–1558.

[10] E. A. Pinilla, J. M. Diaz, J. Coca, *Can. J. Chem. Eng.* **1984**, *62 (5)*, 617–622. DOI: 10.1002/cjce.5450620507

[11] A. Chakma, E. Chornet, R. P. Overend, W. H. Dawson, *Can. J. Chem. Eng.* **1990**, *68 (4)*, 592–598. DOI: 10.1002/cjce.5450680409

[12] J. Kuntz, A. Aroonwilas, *Energy Procedia* **2009**, *1 (1)*, 205–209. DOI: 10.1016/j.egypro.2009.01.029

[13] J. G. Sartori, D. W. Savage, *Ind. Eng. Chem. Fundam.* **1983**, *22 (2)*, 239–249. DOI: 10.1021/i100010a016

[14] P. V. Danckwerts, *Gas Liquid Reactions*, 1st ed., McGraw-Hill Book Company, New York **1970**.

[15] H. Hikita, H. Asai, H. Ishikawa, M. Honda, *Chem. Eng. J.* **1977**, *13 (1)*, 7–12. DOI: 10.1016/0300-9467(77)80002-6

[16] G. F. Versteeg, W. P. M. Van Swaaij, *J. Chem. Eng. Data* **1988**, *33 (1)*, 29–34. DOI: 10.1021/je00051a011

[17] E. D. Snijder, M. J. M. te Riele, G. F. Vertseeg, W. P. M. Van Swaaij, *J. Chem. Eng. Data* **1993**, *38 (3)*, 475–480. DOI: 10.1021/je00011a037

[18] R. Maceira, E. Alvarez, M. Angeles Cancela, *Chem. Eng. J.* **2008**, *138 (1–3)*, 295–300. DOI: 10.1016/j.cej.2007.05.049

[19] T. Elperin, A. Fominykh, *Atmos. Environ.* **2005**, *39 (25)*, 4575–4582. DOI: 10.1016/j.atmosenv.2005.04.005

[20] J. Adam, *Phys. Rep.* **2002**, *356*, 229–365.

[21] N. Roth, K. Anders, A. Frohn, *J. Laser Appl.* **1990**, *2 (1)*, 37. DOI: 10.2351/1.4745251

[22] S. Saengkaew, T. Charinpanikul, C. Laurent, Y. Biscos, G. Lavergne, G. Gouesbet, G. Gréhan, *Exp. Fluids* **2010**, *48 (1)*, 111–119. DOI: 10.1007/s00348-009-0717-3

[23] J. Van Beeck, D. Giannoulis, L. Zimmer, M. Riethmuller, *Opt. Lett.* **1999**, *24 (23)*, 1696–1698. DOI: 10.1364/OL.24.001696

[24] S. Saengkaew, G. Godard, J. B. Blaisot, G. Grehan, *Exp. Fluids* **2009**, *47 (4–5)*, 839–848. DOI: 10.1007/s00348-009-0680-z

[25] S. Saengkaew, *Ph. D. Thesis*, Université de Rouen, France **2006**.

[26] S. Saengkaew, T. Charinpanitkul, H. Vanisri, W. Tanthapanichakoon, L. Mees, G. Gouesbet, G. Grehan, *Opt. Commun.* **2006**, *259 (1)*, 7–13. DOI: 10.1016/j.optcom.2005.08.031

[27] M. R. Vetrano, S. Gauthier, J. van Beeck, P. Boulet, J.-M. Buchlin, *Exp. Fluids* **2006**, *40*, 15–22. DOI: 10.1007/s00348-005-0042-4

[28] X. Wu, Y. Wu, S. Saengkaew, S. Meunier-Guttin-Cluzel, G. Gréhan, L. Chen, K. Cen, *Meas. Sci. Technol.* **2012**, *23 (12)*. DOI: 10.1088/0957-0233/23/12/125302

[29] M. Ouboukhlik, S. Saengkaew, M.-C. Fournier-Salaün, L. Estel, G. Gréhan, *Can. J. Chem. Eng.* **2015**, *93 (2)*, 419–426. DOI: 10.1002/cjce.22123

[30] F. Durst, G. Brenn, T. H. Xu, *Meas. Sci. Technol.* **1997**, *8 (11)*, 1203. DOI: 10.1088/0957-0233/8/11/002

Research Article: The global rainbow technique (GRT) is a non-intrusive way to measure the refractive index of a small volume located in a spray. During CO_2 capture, the concentration and temperature inside the droplet change, leading to an evolution of droplets density, and thus the refractive index. GRT is an effective way to determine the mass transfer extent during absorption with chemical reaction in a spray.

Mass Transfer Evolution in a Reactive Spray during Carbon Dioxide Capture

M. Ouboukhlik*, G. Godard, S. Saengkaew, M.-C. Fournier-Salaün, L. Estel, G. Grehan

Chem. Eng. Technol. **2015**, *38 (XX)*, XXX … XXX

DOI: 10.1002/ceat.201400651

Supporting Information available online